European Journal of Medicinal Chemistry 193 (2020) 112204

Contents lists available at ScienceDirect

European Journal of Medicinal Chemistry

journal homepage: http://www.elsevier.com/locate/ejmech

Research paper

Design, preparation and evaluation of different branched biotin modified liposomes for targeting breast cancer

Baolan Tang [a], Yao Peng [a], Qiming Yue [a], Yanchi Pu [a], Ru Li [a], Yi Zhao [b], Li Hai [a], Li Guo [a, **], Yong Wu [a, *]

[a] Key Laboratory of Drug-Targeting and Drug Delivery System of the Education Ministry and Sichuan Province, Sichuan Engineering Laboratory for Plant-Sourced Drug and Sichuan Research Center for Drug Precision Industrial Technology, West China School of Pharmacy, Sichuan University, Chengdu, 610041, China

[b] Department of Translational Medicine Center, The First Affiliated Hospital of Zhengzhou University, Zhengzhou, 450052, China

ARTICLE INFO

Article history:
Received 27 December 2019
Received in revised form
2 March 2020
Accepted 2 March 2020
Available online 5 March 2020

Keywords:
Biotin
Active targeting ligand
Breast cancer
Drug delivery
Liposome

ABSTRACT

A series of liposome ligands (Bio-Chol, Bio-Bio-Chol, tri-Bio-Chol and tetra-Bio-Chol) modified by different branched biotins that can recognize the SMVT receptors over-expressed in breast cancer cells were synthesized. And four liposomes (Bio-Lip, Bio-Bio-Lip, tri-Bio-Lip and tetra-Bio-Lip) modified by above mentioned ligands as well as the unmodified liposome (Lip) were prepared to study the targeting ability for breast cancer. The cytotoxicity study and apoptosis assay of paclitaxel-loaded liposomes showed that tri-Bio-Lip had the strongest anti-proliferative effect on breast cancer cells. The cellular uptake studies on mice breast cancer cells (4T1) and human breast cancer cells (MCF-7) indicated tri-Bio-Lip possessed the strongest internalization ability, which was 5.21 times of Lip, 2.60 times of Bio-Lip, 1.67 times of Bio-Bio-Lip and 1.17 times of tetra-Bio-Lip, respectively. Moreover, the 4T1 tumor-bearing BALB/c mice were used to evaluate the *in vivo* targeting ability. The data showed the enrichment of liposomes at tumor sites were tri-Bio-Lip > tetra-Bio-Lip > Bio-Bio-Lip > Bio-Lip > Lip, which were consistent with the results of *in vitro* targeting studies. In conclusion, increasing the density of targeting molecules on the surface of liposomes can effectively enhance the breast cancer targeting ability, and the branching structure and spatial distance of biotin residues may also have an important influence on the affinity to SMVT receptors. Therefore, tri-Bio-Lip could be a promising drug delivery system for targeting breast cancer.

1. Introduction

According to the latest WHO statistics, breast cancer as a highly heterogeneous systemic disease is the leading threaten of cancers in women worldwide, with high incidence and high mortality [1]. Despite significant progress has been made in the breast cancer treatment during the past decades, the current therapeutic effect is still far from optimal outcomes. Surgery, radiotherapy, chemotherapy and hormone therapy are the regular clinical approaches, yet they have the disadvantages of low specificity and inevitably severe side effects [2,3].

Nanomedicine is a promising alternative for breast cancer treatment in contrast to basic therapeutic approaches. Chemotherapeutic agents have been reformulated into liposomes or nanoparticle which improve accumulation within the tumor site. For example, the commercial availability of Doxil® and Abraxane® have been extensively used for breast cancer adjuvant therapy [4]. However, these nanomedicines can only be passively enriched in tumor sites through the enhanced permeability and retention effect (EPR effect), which were originally designed to be broad-spectrum anticancer agents rather than specific for breast cancer treatment. Thus, their therapeutic effect for breast cancer are barely satisfactory. For these reasons, finding novel targeting drug delivery systems (TDDS) are the focus of current researches on breast cancer treatment.

As drug carriers, nanomaterials have many advantages in cancer treatment, such as easy surface modification, adjustable particle size and surface charge, high porosity and large specific surface area etc [5–10]. At present, many kinds of TDDS have been applied to the

* Corresponding author.
** Corresponding author.
E-mail addresses: guoli@scu.edu.cn (L. Guo), wyong@scu.edu.cn (Y. Wu).

https://doi.org/10.1016/j.ejmech.2020.112204
0223-5234/

treatment for breast cancer, like micelles, albumin, and gold nanoparticles [11–17]. Among these nanocarriers, liposome is considered to be the most mature TDDS, which has similar biological structure to cell membrane, good biocompatibility and safety [18–21].

The surface ligand functionalization of nanocarriers directly affects the targeting ability of TDDS, which has long been considered as a crucial factor for the targeting efficiency. So far, many types of ligands (e.g., cyclic RGD, folic acid, biotin, hyaluronic acid, human epidermal receptor 2, galactose, glycyrrhizin and bisphosphonates) have been employed for active tumor-targeting drug delivery [22–24]. For example, biotin, as a water-soluble small molecule (244 Da) vitamin that can not be synthesized by human or any mammalian cells [25–27], has great advantages such as simple structure, single functional group, smaller steric hindrance, and easy to be modified on the surface of nanocarriers. Moreover, the sodium-dependent multivitamin transporter (SMVT) has been proved to be the main transporter of biotin [28,29]. It has been reported that SMVT was overexpressed in several aggressive cancer lines such as breast cancer (MCF-7, 4T1, JC, MMT06056), while at low levels in normal cells [30–33]. These evidences suggest that biotin would be a promising ligand for targeting breast cancer.

Along with the functionalization of surface ligands on nanocarriers, researchers have focused on the modification of ligands. And few studies have been carried out on the density of ligand residues on the surface of nanocarriers, which is also essential for ligands to enhance their targeting ability, for example, increasing the percentage of single-branched modified nanomaterials, using multi-branched ligand modified nanomaterial and so on. Moreover, multi-branched ligand seems more promising compared with the single-branched ligand. For instance, Wu's group explored multivalent glucosides with high affinity as ligands for brain targeting liposomes [34]; and Zhang's group studied the targeting efficiency of RGD-modified nanocarriers with different ligand intervals in response to integrin $a_v\beta_3$ clustering [35]; in addition, Punit P. Seth used triantennary *N*-acetylgalactosamine conjugated antisense oligonucleotides for targeted delivery to hepatocytes [36]. All of the three examples used the branched ligands to modify the nanocarriers and made a great breakthrough.

In our previous study, we have synthesized ligands Bio-Chol, Bio-Bio-Chol modified by biotin (Fig. 1), and preliminarily discussed the density of targeting molecular and different ligand modification methods on the targeting ability of liposomes for breast cancer [37]. The results showed that increasing the density of targeting molecules on the surface of liposomes for SMVT recognition can effectively enhance the targeting ability of liposomes for breast cancer; furthermore, at the same density of targeting molecules, liposomes modified by branched ligand had stronger breast cancer targeting ability. But there is still a lot of room to explore and improve the breast targeting ability of branched biotin modified liposomes.

Based on our previous study, tri-Bio-Chol and tetra-Bio-Chol modified by biotin with different branches were designed and synthesized in this paper (Fig. 1). And different types of biotin-modified liposomes were prepared by lipid film hydration-ultrasound method using paclitaxel (PTX) as a model drug for breast cancer targeting study *in vitro* and *in vivo*.

2. Materials and methods

2.1. Materials

All liquid reagents were distilled before use. All unspecified reagents were from commercial resources. TLC was performed using precoated silica gel GF254 (0.2 mm), while column chromatography was performed using silica gel (100–200 mesh). ^{1}H NMR spectra were taken on a Varian INOVA 400 or 600 (Varian, Palo Alto, CA, USA) using $CDCl_3$ or DMSO-d_6 as solvent. Chemical shifts are expressed in δ (ppm), with tetramethylsilane (TMS) functioning as the internal reference, and coupling constants (J) were expressed in Hz. Paclitaxel were obtained from National Institute for Food and Drug Control. Soybean phospholipids (SPC) were purchased from Kelong Chemical (Chengdu, China). Cholesterol (Chol) was purchased from Bio Life Science & Technology Co., Ltd (Shanghai, China). D-(+)-Biotin was purchased from Shanghai Darui Finechemical Co., Ltd (Shanghai, China). 1, 2-dioleoyl-snglycero-3-phosphoethanolamine-N-(carboxyfluorescein) (CFPE) were purchased from Avanti Polar Lipids (USA). 4′-6-Diamidino-2-phenylindole (DAPI) and 3-(4, 5-Dimethylthiazol-2-yl)-2, 5-diphenyltetrazolium bromide (MTT) were purchased from Beyotime Institute Biotechnology (Haimen, China). 4-chlorobenzenesulfonate salt (DiD) were purchased from Biotium (USA). Annexin V-FITC/PI apoptosis detection kit was obtained from KeyGEN Biotech (China).

2.2. Synthesis of ligands

2.2.1. Synthesis of ligand ***Bio-Chol*** *and ligand* ***Bio-Bio-Chol***

The synthesis of ligand **Bio-Chol** and ligand **Bio-Bio-Chol** was reported in our previous work [37].

2.2.2. Synthesis of compound ***2–5***

The synthesis of compound **2**–**5** was reported in our previous work [37,38].

2.2.3. Synthesis of compound ***7***

Diethanolamine **6** (1.00 g, 9.51 mmol) was dissolved in 30 mL acetonitrile, and tert-butoxycarbonyl anhydride (2.49 g, 11.41 mmol) was added under room temperature agitation. After stirring for 4 h at room temperature, the mixture was concentrated in vacuo. The residue was purified by flash column chromatography to afford compound **7** (1.82 g, 93%) as a colorless oil. ^{1}H NMR (400 MHz, $CDCl_3$, ppm) δ: 3.80 (s, 4H), 3.44 (d, 4H, $J = 11.6$ Hz), 2.83 (s, 2H), 1.47 (s, 9H).

2.2.4. Synthesis of compound ***8***

To a solution of D-(+)-Biotin (2.38 g, 9.76 mmol) in mixed solvent of 45 mL dichloromethane and 15 mL N, *N*-dimethylformamide was added 1-Ethyl-3-(3-dimethylaminopropyl)carbodiimide hydrochloride (EDCI, 2.80 g, 14.61 mmol), DMAP (1.78 g, 14.61 mmol) and *N, N*-Diisopropylethylamine (DIPEA, 4.84 mL, 29.28 mmol) at room temperature, then compound **7** (500 mg, 2.44 mmol) in 10 mL dichloromethane was added slowly. After stirring for 10 h, the mixture was washed with 1 mol/L HCl and saturated NaCl. The organic layer was dried over anhydrous Na_2SO_4, filtered and concentrated in vacuo. The residue was purified by flash column chromatography to afford compound **8** (1.24 g, 77%) as a yellowish solid; mp: 108–110 °C. ^{1}H NMR (400 MHz, $CDCl_3$, ppm) δ: 4.54–4.52 (m, 2H), 4.35 (s, 2H), 4.19 (s, 4H), 3.54–3.43 (m, 4H), 3.18–3.12 (m, 2H), 2.95–2.90 (m, 2H), 2.75 (d, 2H, $J = 7.2$ Hz), 2.38 (s, 4H), 1.76–1.65 (m, 8H), 1.47 (s, 9H), 1.29–1.26 (m, 4H).

2.2.5. Synthesis of compound ***9***

Compound **8** (3.22 g, 5.77 mmol) was dissolved in 20 mL dichloromethane, and then trifluoroacetic acid (10 mL) was added under room temperature agitation. After stirring for 4 h at room temperature, the mixture was concentrated in vacuo to afford 3.47 g dark green oil, then 30 mL of ice ether was added to separate out the yellowish solid. After centrifugation and drying, 2.94 g compound **9** as a yellowish solid was obtained.

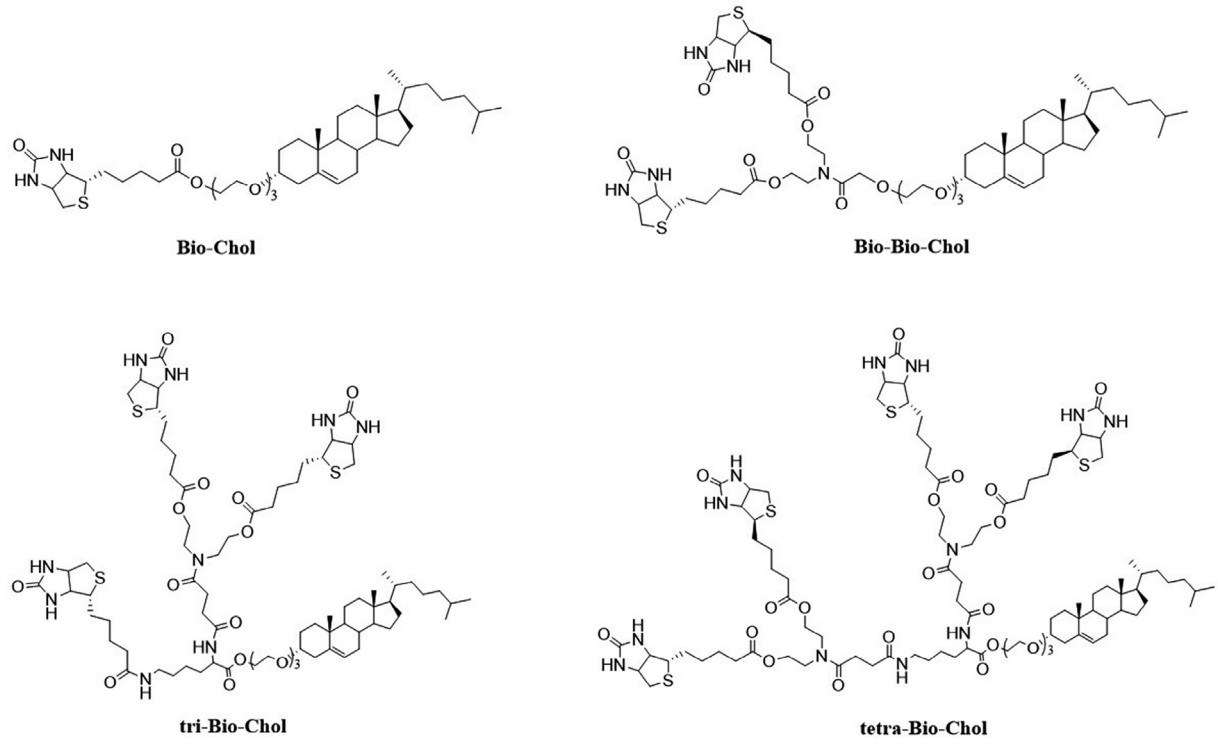

Fig. 1. The structure of ligands Bio-Chol, Bio-Bio-Chol, tri-Bio-Chol and tetra-Bio-Chol.

*2.2.6. Synthesis of compound **10***

To a mixture of succinic anhydride (1.12 g, 11.2 mmol) and dichloromethane (25 mL), triethylamine (3.12 mL, 22.4 mmol) and the solution of compound **9** (3.76 g, 5.59 mmol) in 45 mL dichloromethane were added at room temperature subsequently. After stirring for 6 h, the mixture was washed with 1 mol/L HCl and saturated NaCl. The organic layer was dried over anhydrous Na_2SO_4, filtered and concentrated in vacuo. The residue was purified by flash column chromatography to afford compound **10** (2.14 g, 58%) as a colorless oil. ^{1}H NMR (400 MHz, $CDCl_3$, ppm) δ: 12.09 (br, 1H), 4.33–4.29 (m, 2H), 4.19–4.12 (m, 4H), 4.09–4.06 (m, 2H), 3.61 (t, 2H, J = 5.6 Hz), 3.50 (t, 2H, J = 5.6 Hz), 3.18–3.12 (m, 2H), 3.10 (s, 2H), 2.85–2.80 (m, 2H), 2.59–2.56 (m, 4H), 2.50 (s, 4H), 2.44–2.41 (m, 2H), 1.64–1.42 (m, 8H), 1.37–1.26 (m, 4H).

*2.2.7. Synthesis of compound **11***

To a solution of compound **10** (1.16 g, 1.76 mmol) in mixed solvent of 40 mL dichloromethane and 10 mL N, *N*-dimethylformamide was added 2-(7-aza-1H-benzotriazole-1-yl)-1,1,3,3-tetramethyluronium hexafluorophosphate (HATU, 802 mg, 2.11 mmol) and DIPEA (873 μL,5.28 mmol) at −5 °C, and the reaction was stirred at the temperature for 30 min. Then compound **5** (876 mg, 1.17 mmol) in 12 mL dichloromethane was added slowly. After stirring for another 6 h, the mixture was washed with 1 mol/L HCl and saturated NaCl. The organic layer was dried over anhydrous Na_2SO_4, filtered and concentrated in vacuo. The residue was purified by flash column chromatography to afford compound **11** (1.32 g, 81%) as a pale yellow jelly. ^{1}H NMR (600 MHz, $CDCl_3$, ppm) δ: 5.34 (s, 1H), 4.57–4.09 (m, 11H), 3.75–3.39 (m, 14H), 3.20–3.15 (m, 3H), 3.07 (t, 2H, J = 6.0 Hz), 2.92–2.66 (m, 8H), 2.36 (d, 4H, J = 10.2 Hz), 2.23–0.86 (remaining cholesterol & lys & biotin protons), 1.44 (s, 9H), 0.99 (s, 3H), 0.92 (d, 3H, J = 6.6 Hz), 0.87 (d, 6H, J = 6.0 Hz), 0.68 (s, 3H).

*2.2.8. Synthesis of compound **12***

Compound **11** (600 mg, 0.43 mmol) was dissolved in 6 mL dichloromethane, and 2 mL trifluoroacetic acid was added under room temperature agitation. After stirring for 30 min at room temperature, the mixture was washed with saturated $NaHCO_3$ and NaCl. The organic layer was dried over anhydrous Na_2SO_4, filtered and concentrated in vacuo to afford compound **12** (525 mg, 94%) as pale yellow jelly. ^{1}H NMR (600 MHz, $CDCl_3$, ppm) δ: 5.35 (s, 1H), 4.54–4.06 (m, 11H), 3.72–3.42 (m, 14H), 3.18–3.12 (m, 3H), 2.92–2.66 (m, 10H), 2.37–2.32 (m, 4H), 2.29–0.86 (remaining cholesterol & lys & biotin protons), 1.44 (s, 9H), 0.99 (s, 3H), 0.91 (d, 3H, J = 10.2 Hz), 0.86 (d, 6H, J = 10.8 Hz), 0.67 (s, 3H).

*2.2.9. Synthesis of ligand **tri-Bio-Chol***

To a solution of D-(+)-Biotin (150 mg, 0.61 mmol) in mixed solvent of 24 mL dichloromethane and 8 mL N, *N*-dimethylformamide was added HATU (278 mg, 0.73 mmol) and DIPEA (202 μL, 1.22 mmol) at −5 °C. After the reaction was stirred at the temperature for 30 min, compound **12** (525 mg, 0.41 mmol) in 13 mL dichloromethane was added slowly. After stirring for another 10 h, the mixture was washed with 1 mol/L HCl and saturated NaCl. The organic layer was dried over anhydrous Na_2SO_4, filtered and concentrated in vacuo. The residue was purified by flash column chromatography to afford ligand tri-Bio-Chol (521 mg, 84%) as a pale yellow solid; mp: 121–123 °C. ^{1}H NMR (600 MHz, $CDCl_3$, ppm) δ: 5.34 (s, 1H), 4.54–4.05 (m, 13H), 3.92–3.52 (m, 14H), 3.20–3.16 (m, 6H), 2.91–2.72 (m, 10H), 2.36 (d, 4H, J = 12.0 Hz), 2.24–0.86 (remaining cholesterol & lys & biotin protons), 0.99 (s, 3H), 0.91 (d, 3H, J = 6.0 Hz), 0.87 (d, 3H, J = 6.6 Hz), 0.68 (s, 3H). HR-MS calculated for $C_{77}H_{125}N_9O_{15}S_3Na$ $[M+Na]^+$ 1534.8426, found 1534.8431.

*2.2.10. Synthesis of ligand **tetra-Bio-Chol***

To a solution of compound **10** (408 mg, 0.62 mmol) in 10 mL

dichloromethane was added HATU (354 mg, 0.93 mmol) and DIPEA (308 μL, 1.86 mmol) at −5 °C. The reaction was stirred at the temperature for 30 min, and then compound **12** (397 mg, 0.31 mmol) in 10 mL dichloromethane was added slowly. After stirring for another 10 h, the mixture was washed with 1 mol/L HCl and saturated NaCl. The organic layer was dried over anhydrous Na_2SO_4, filtered and concentrated in vacuo. The residue was purified by flash column chromatography to afford ligand **tetra-Bio-Chol** (415 mg, 70%) as a pale yellow solid; mp: 154–157 °C. ^{1}H NMR (600 MHz, $CDCl_3$, ppm) δ: 5.34 (s, 1H), 4.55–4.04 (m, 19H), 3.90–3.40 (m, 18H), 3.19–3.14 (m, 7H), 2.90–2.61 (m, 14H), 2.37–2.33 (m, 10H), 2.27–0.86 (remaining cholesterol & lys & biotin protons), 0.99 (s, 3H), 0.91 (d, 3H, J = 6.6 Hz), 0.87 (d, 3H, J = 6.6 Hz), 0.68 (s, 3H). HR-MS calculated for $C_{95}H_{152}N_{12}O_{21}S_4Na$ $[M+Na]^+$ 1949.0037, found 1949.0052.

2.3. Preparation and characterization of liposomes

Liposomes were prepared by thin film hydration method. Lipid composition of the liposomes was as follows: soybean phospholipid (SPC)/cholesterol/ligand = 64/33/3 (molar ratio). All lipid materials were dissolved in a mixture solvent chloroform/methanol (v/v = 2/1), and then the organic solvent was removed by rotary evaporation to form a lipid film. After overnight in vacuum, the obtained film was hydrated in PBS (pH 7.4) at 20 °C for 0.5 h. Liposomes were then formed by further intermittent sonication at 80 W for 3 min by a probe sonicator.

PTX-loaded liposomes were prepared by adding paclitaxel to the lipid organic solution prior to the evaporation of solvent. Likewise, CFPE-labeled liposomes and DiD-loaded liposomes were prepared by adding appropriate amount of CFPE or DiD to the solution respectively. The entrapment efficiency of paclitaxel was determined by HPLC (Shimadzu, Kyoto, Japan). The average particle size and zeta potential of Lip, Bio-Lip, Bio-Bio-Lip, tri-Bio-Lip and tetra-Bio-Lip were measured using Malvern Zeta sizer Nano ZS90 (Malvern Instruments Ltd., U.K).

2.4. In vitro drug release study

In vitro paclitaxel release study was performed using dialysis method. Free PTX was prepared as follows: PTX was dissolved in a mixture of ethanol-Cremophor ELP35 with a volume ratio of 1:1. Each PTX-loaded liposome (0.4 mL) or free paclitaxel was placed in an 8000–14000 Da dialysis bag and sealed. Then the dialysis bags were incubated in 40 mL PBS containing 0.1% (v/v) Tween 80 at 37 °C for 48 h with oscillating at 45 rpm. At 0 h, 1 h, 2 h, 4 h, 8 h, 12 h, 24 h and 48 h, 0.1 mL release medium was sampled and replaced with equal volume of fresh release medium. Then the samples were diluted with acetonitrile and the concentrations of paclitaxel were measured at the wavelength of 227 nm by HPLC.

2.5. In vitro stability of liposomes in serum

The serum stability of the liposomes was conducted by the turbidimetric method. Briefly, liposomes were mixed with an equal volume of fetal bovine serum (FBS) under 37 °C with moderate agitation at 45 rpm. Samples were taken at predetermined time points (0 h, 1 h, 2 h, 4 h, 8 h, 12 h, 24 h and 48 h), and the transmittance was measured at 750 nm by a microplate reader (Thermo Scientific Varioskan Flash, USA).

2.6. Hemolysis assays

Hemolysis assays were performed to assess the biosecurity of liposomes during the blood circulation. Fresh mouse blood was collected in tubes containing heparin sodium. The red blood cells (RBCs) were separated and collected by centrifugation at 5×10^3 rpm for 10 min and washed with PBS until the supernatant became colorless. Subsequently, the RBCs were diluted with PBS to a concentration of 2% (v/v). Various concentrations (10, 25, 50, 100, 200 300, 400 μmol/L) of liposomes were co-incubated with equal volume of 2% RBCs solutions for 1 h at 37 °C with moderate shaking. After centrifugation at 10000 rpm for 10 min, the absorbance of hemoglobin was measured using a microplate reader at 540 nm. The values for 0% and 100% hemolysis were determined by incubating erythrocytes with PBS or 1% (v/v) Triton X-100. The hemolysis percentage was calculated using the following equation:

$$\text{The percent hemolysis} = \frac{ASample - ANegative}{APostive - ANegative} \times 100\%$$

where A is the absorbance of hemoglobin.

2.7. Cytotoxicity

The cytotoxicity of PTX-loaded liposomes and free PTX against 4T1 cells and MCF-7 cells (the biotin receptor positive cell lines) as well as the normal cell line L929 cells were measured with MTT assay. Generally, the cells were seeded in a 96-well plate at a density of 5×10^3 cells/well and cultured for 24 h at 37 °C. PTX-loaded liposomes and free paclitaxel were diluted to concentrations of 20 μg/mL、5 μg/mL、1 μg/mL、0.5 μg/mL、0.1 μg/mL and 0.01 μg/mL with medium, and added into each well. After incubation for 48 h, 20 μL MTT solutions (5.0 mg/mL) was added to the wells and incubated for another 4 h at 37 °C. After removal of the culture medium, the reduced MTT dye was solubilized by DMSO (150 μL) and the absorbance was read at 490 nm wavelength by an automatic microplate spectrophotometer. Cells with drug-free medium were used as control. Cell viability (%) was calculated as the following equation: $A_{test}/A_{control} \times 100\%$, where A_{test} and $A_{control}$ represented the absorbance of treated cells and control cells, respectively.

2.8. Apoptosis assay

To evaluate the cell apoptosis induced by PTX-loaded liposomes and free PTX, 4T1 cells were treated with PTX-loaded liposomes and free PTX (PTX concentration of 0.01 μg/mL) for 24 h under 37 °C. And then, cells were harvested, washed three times with cold PBS and resuspended in 500 μL binding buffer. Then 5 μL Annexin V-FITC and 5 μL PI were added and incubated with the cells for 15 min in the dark. Finally, the stained cells were analyzed by a flow cytometer (BD FACSCelesta, BD, USA). PTX-Lip group was set as control.

2.9. Cellular uptake

4T1 cells and MCF-7 cells were seeded in 12-well plates at a density of 3×10^5 cells/well and cultured for 24 h at 37 °C. CFPE-labeled different liposomes were added into each well with a final concentration of CFPE at 2 μg/mL. After cultured for 4 h at 37 °C, trypsin was used to harvest the cells, which were washed three times with PBS afterward, and finally resuspended in 0.3 mL PBS. Then, the fluorescent intensity of cells was measured by a flow cytometer.

For qualitative experiments, 4T1 cells and MCF-7 cells were plated onto a 6-well plate containing cover glass at a density of 3×10^5 cells/well and cultured for 24 h at 37 °C. CFPE-labeled liposomes were added into each well with a final concentration of CFPE at 2 μg/mL and allowed for further co-incubation for 4 h.

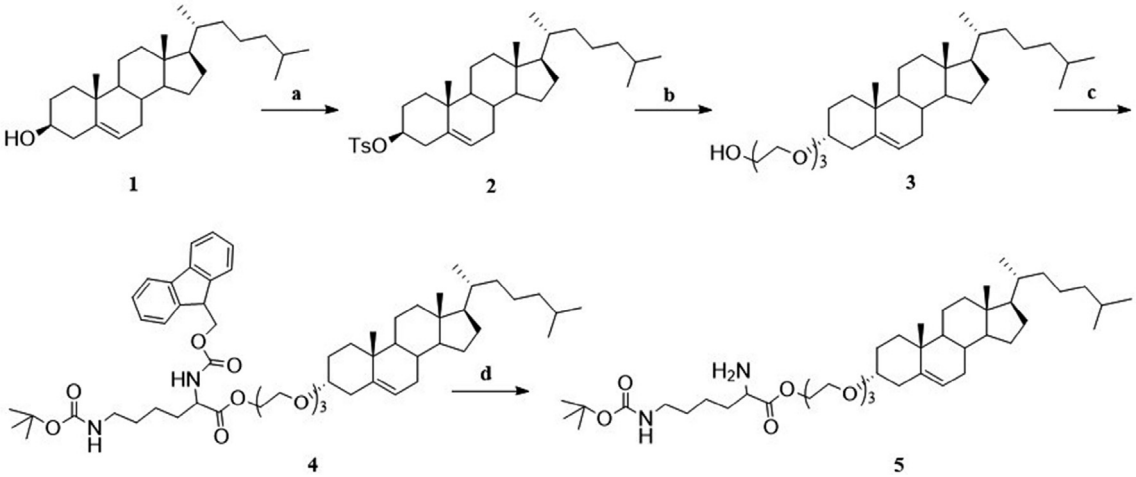

Scheme 1. The synthetic route of cholesteric component. Reagents and conditions: (a) TsCl, pyridine, 50 °C, 5 h; (b) Triethylene glycol, dioxane, reflux, 6 h; (c) *N*-Boc-*N'*-Fmoc-L-Lysine, DCC, DMAP, CH_2Cl_2, -5 °C- r.t., 8 h; (d) DBU, CH_2Cl_2, r.t., 20 min.

Following that, the cells were rinsed with cold PBS three times and fixed with 4% paraformaldehyde for 30 min at room temperature, and then cell nuclei were stained with DAPI (0.1 μg/mL) for 5 min. Finally, the samples were imaged using laser scanning confocal microscope (CLSM) (LSM800, Carl Zeiss AG, Germany).

2.10. In vivo imaging

Tumor targeting capability of DiD-loaded liposomes Lip, Bio-Lip, Bio-Bio-Lip, tri-Bio-Lip and tetra-Bio-Lip was investigated in subcutaneous 4T1 breast tumor model [39]. Briefly, the female BALB/c mice were subcutaneously injected with 0.1 mL of cell suspension containing 2×10^7 4T1 cells/mL in the right flank at day 0. After 14 days, the mice were randomly divided into five groups and were intravenously injected via the caudal vein with DiD-loaded liposomes at a dose of 200 μg/kg DiD. Then, the mice were anesthetized with 4% chloral hydrate and imaged with IVIS Lumina Series III imaging system (LIVIS Lumina III, Perkin Elmer, USA) at 1 h, 4 h, 8 h, 12 h and 24 h after injection. The mice were sacrificed after heart perfusion with saline. Tumors, hearts, livers,

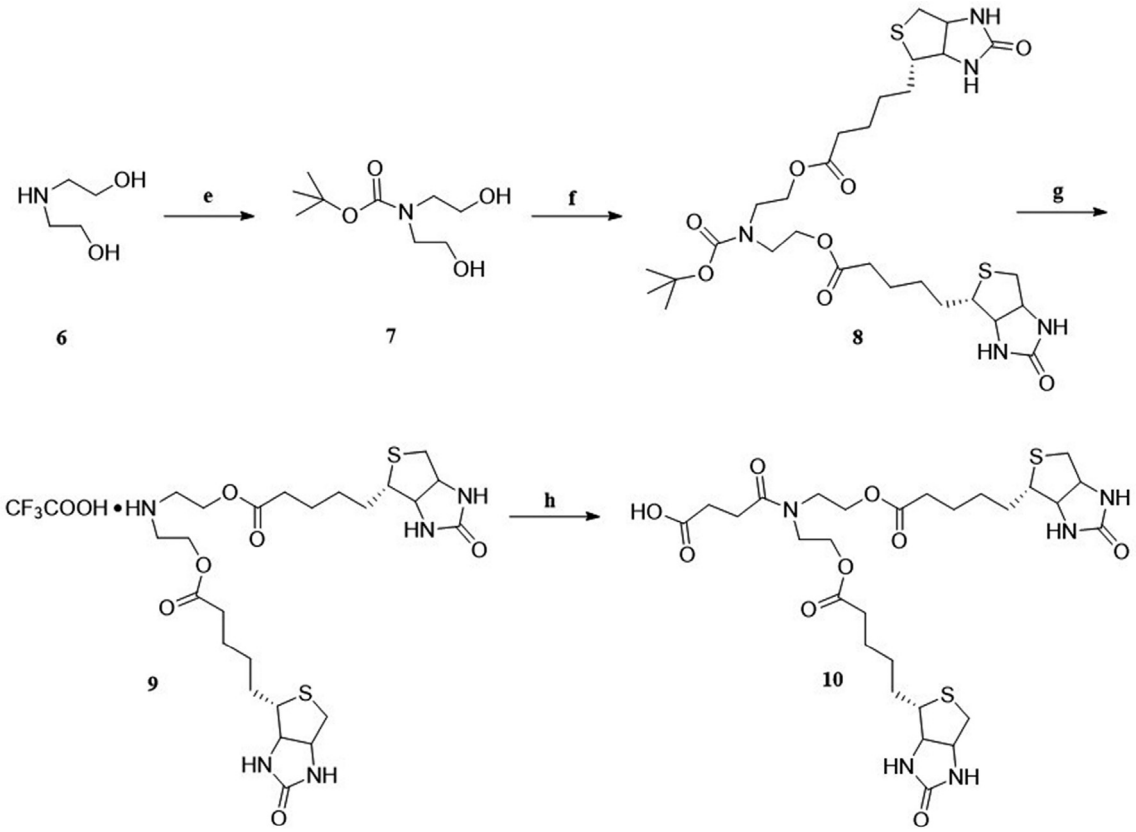

Scheme 2. The synthetic route of targeted component. Reagents and conditions: (e) $(Boc)_2O$, CH_3CN, r.t., 4 h; (f) Biotin, EDCI, DMAP, CH_2Cl_2,r.t., 10 h; (g) CF_3COOH, CH_2Cl_2, r.t., 4 h; (h) Et_3N, succinic anhydride, CH_2Cl_2, r.t., 6 h.

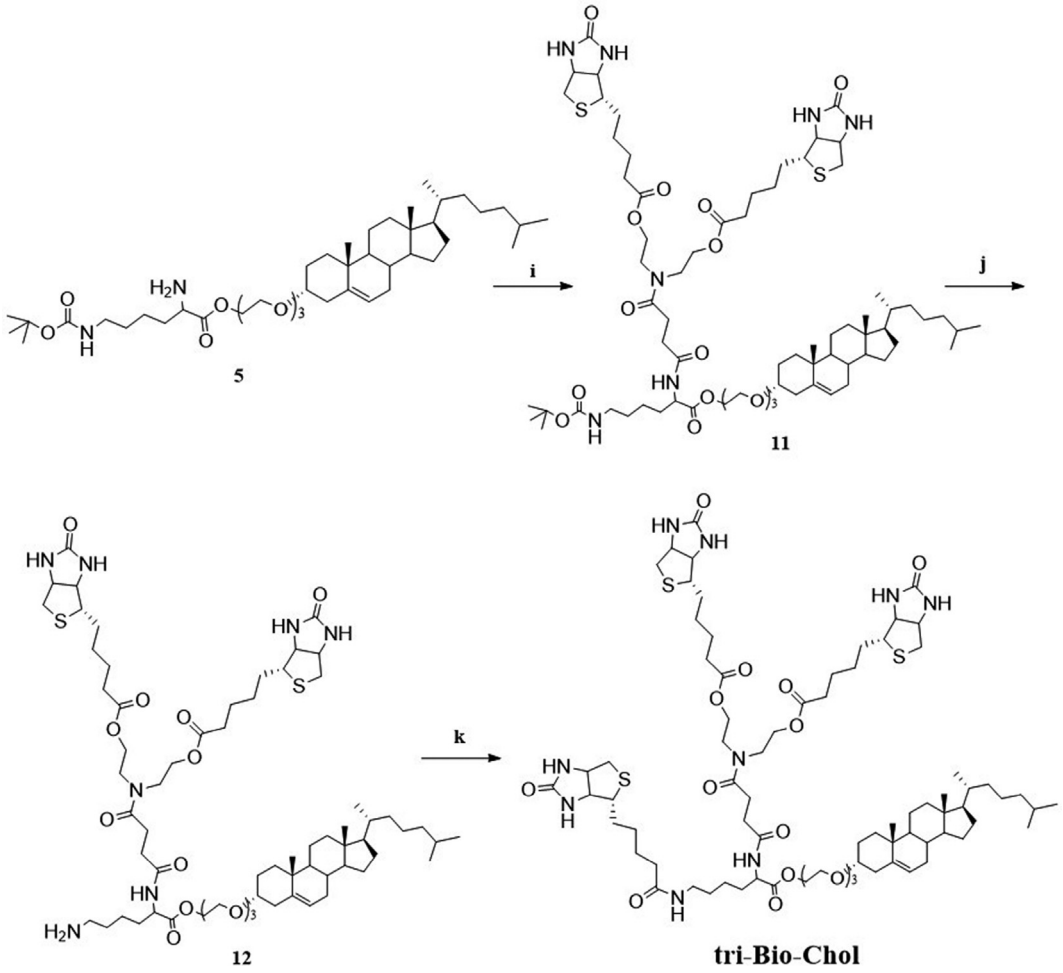

Scheme 3. The synthetic route of ligand tri-Bio-Chol. Reagents and conditions: (i) Compound **10**, HATU, DIPEA, CH_2Cl_2, r.t., 6 h; (j) CF_3COOH, CH_2Cl_2, r.t., 30 min; (k) Biotin, HATU, DIPEA, CH_2Cl_2, DMF, −5 °C- r.t., 10 h.

spleens, lungs and kidneys were collected. All the tissues and organs were also imaged with IVIS Lumina Series III imaging system.

2.11. Statistical analysis

Data were analyzed using an F-test with subsequent T-tests (equal variance) for the comparison between two different groups. For 3 or more groups, one-way ANOVA with Tukey's multiple comparison test was used. A value of $p < 0.05$ was considered significant.

3. Results and discussion

3.1. Synthesis of ligand tri-Bio-Chol

The synthetic route of ligand **tri-Bio-Chol** can be divided into three parts: (1) synthesis of cholesteric component (Scheme 1), (2) synthesis of targeted component (Scheme 2), (3) coupling of cholesteric component and targeted component (Scheme 3).

In the first part, compound **3** was synthesized by 2 steps reaction from cholesterol **1**, which was then conjugated with *N*-Boc-*N′*-Fmoc-L-Lysine in the presence of DCC and DMAP to obtain compound **4**, the Fmoc protective group of compound **4** was later removed by DBU to afford compound **5**. In the second part, compound **7** was synthesized by the reaction of diethanolamine with $(Boc)_2O$, then was conjugated with biotin in the presence of EDCI and DMAP to obtain compound **8**. The protective group of compound **8** was subsequently removed and reacted with succinic anhydride to obtain compound **10**.

As shown in Scheme 3, after the cholesteric component and targeted component were synthesized respectively, compound **11** was obtained from compound **5** and compound **10** under the action of the condensation agent HATU. Subsequently, the Boc protection group of compound **11** was removed by CF_3COOH to afford compound **12**, and finally the ligand tri-Bio-Chol was synthesized by condensation of compound **12** with biotin. All the title compounds and important intermedium were characterized by their respective ^1H NMR and MS.

3.2. Synthesis of ligand tetra-Bio-Chol

Scheme 4 showed the synthetic route of ligand **tetra-Bio-Chol**. Firstly, using cholesterol as raw material, compound **11** was obtained by multi-step reaction in accordance with the synthetic method of ligand **tri-Bio-Chol** as described in section 3.1. Then, the protective group of compound **11** was removed by CF_3COOH to afford compound **12**. Finally, compound **10** was conjugated with compound **12** in the presence of HATU and DIPEA to obtain ligand tetra-Bio-Chol.

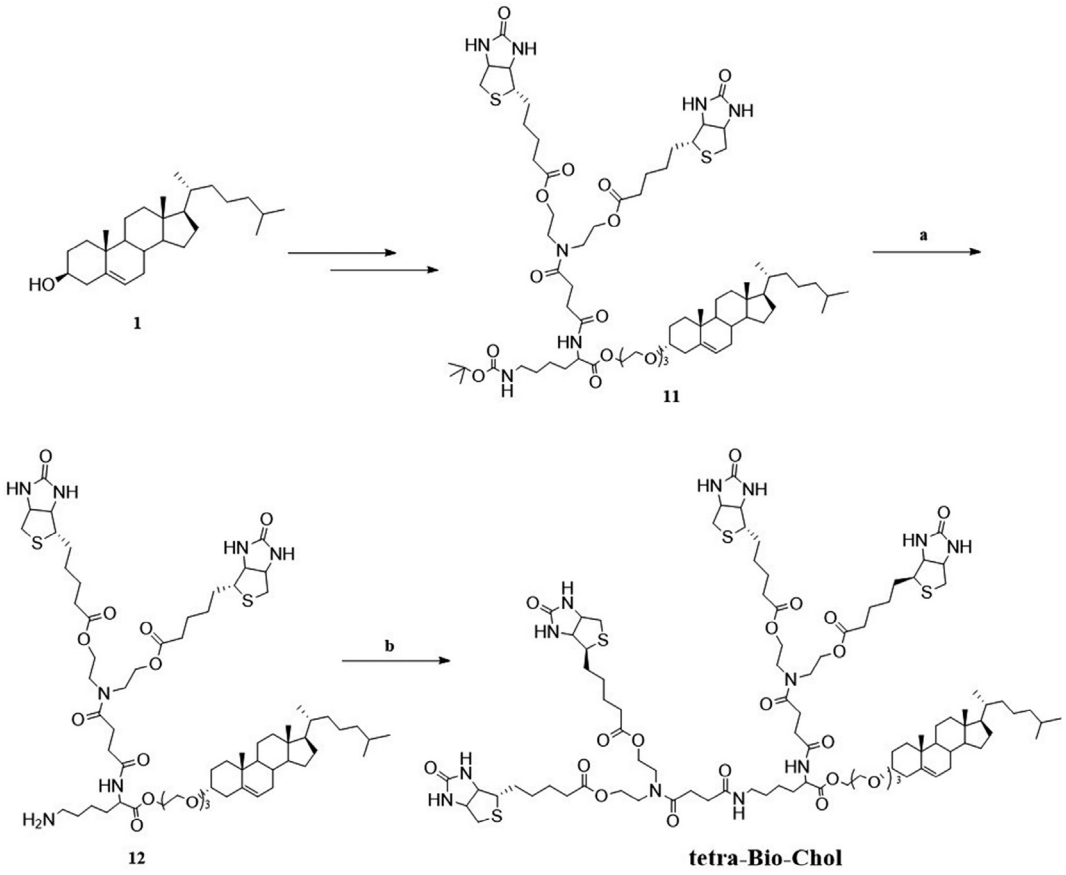

Scheme 4. The synthetic route of ligand tetra-Bio-Chol. Reagents and conditions: (a) CF_3COOH, CH_2Cl_2, r.t., 30 min; (b) Compound **10**, HATU, DIPEA, CH_2Cl_2, DMF, −5 °C- r.t., 10 h.

Table 1
The composition and characterization of different paclitaxel-loaded liposomes (mean ± SD, $n = 3$).

Liposomes	Size(nm)	PDI	EE (%)	Zeta potential (mV)
PTX-Lip	106.8 ± 3.5	0.146 ± 0.025	90.26 ± 2.13	−3.27 ± 0.23
PTX-Bio-Lip	105.3 ± 2.1	0.133 ± 0.019	88.54 ± 3.43	−3.59 ± 0.31
PTX-Bio-Bio-Lip	110.9 ± 3.4	0.128 ± 0.036	87.62 ± 1.77	−2.63 ± 0.14
PTX-tri-Bio-Lip	102.2 ± 2.7	0.119 ± 0.022	89.13 ± 4.37	−2.72 ± 0.41
PTX-tetra-Bio-Lip	113.2 ± 1.9	0.154 ± 0.014	86.78 ± 2.08	−2.33 ± 0.26

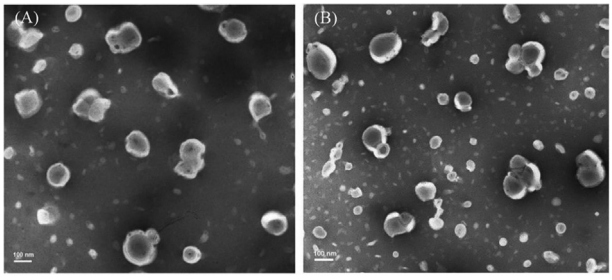

Fig. 2. The TEM image of PTX-tri-Bio-Lip (A) and PTX-tetra-Bio-Lip (B).

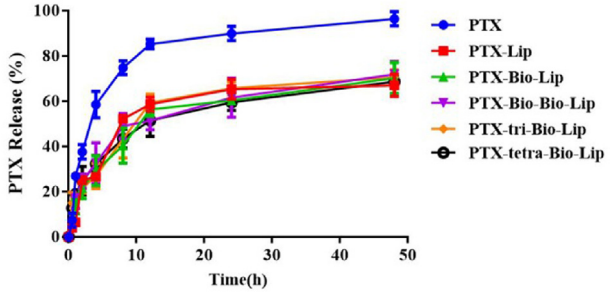

Fig. 3. The PTX release profiles of free PTX and different PTX-loaded liposomes (mean ± SD, $n = 3$).

3.3. Characterization of liposomes

Proper size, uniform distribution, zeta potential, and high encapsulation efficiencies (EE%) of nanoparticles are crucial to reach the targeted site and play their therapeutic effect [40]. As can be seen from Table 1, for all types of liposomes, the PTX were well encapsulated in the liposomes, whose encapsulation efficiencies were all greater than 86%. In addition, the average particle sizes of all liposomes ranged from 102 to 114 nm, and the values of PDI were less than 0.2. Besides, the liposomes were weak negative charged, which is helpful for escaping the absorption of the reticuloendothelial system and immune response. What's more, the

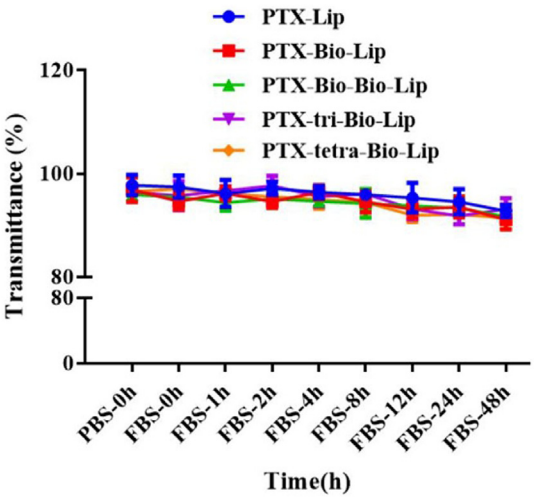

Fig. 4. The variations of transmittance of different PTX-loaded liposomes in 50% FBS (mean ± SD, $n = 3$).

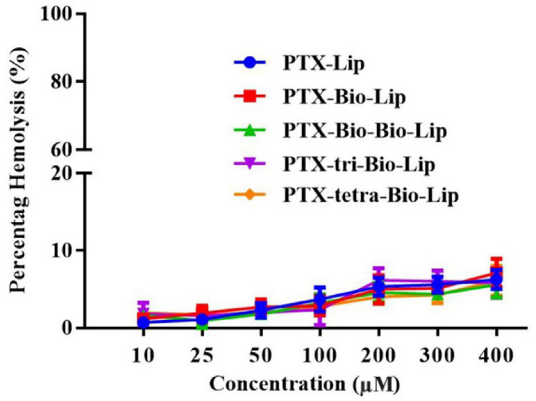

Fig. 5. Hemolysis percentage of different PTX-loaded liposomes (mean ± SD, $n = 3$).

PTX-tri-Bio-Lip and PTX-tetra-Bio-Lip exhibited uniform spherical in shape and suitable size (Fig. 2) under transmission electron microscopy (TEM). The Characterization of liposomes showed the liposomes can accumulate in tumor through EPR effect.

3.4. In vitro drug release study

To mimic the drug release behavior *in vivo*, the PTX-loaded liposomes were co-incubated with 1% Tween 80 in PBS. As shown in Fig. 3, the release of free paclitaxel was relatively rapid, after 12 h of incubation, more than 85% of drugs were released into the medium. The PTX loaded in liposomes was released slowly with no significant sudden release, whose cumulative release amount was less than 72% after 48 h of co-incubation with PBS. The results showed that these PTX-loaded liposomes could improve the drug release behavior and have sustained release effects. With the increase of targeted molecular density, there was no significant difference in the drug release behavior of PTX-loaded liposomes in each group.

3.5. In vitro stability of liposomes in serum

The liposomes must possess appropriate stability in the circulatory system to reach the targeted site. As shown in Fig. 4, within 48 h of co-incubation with 50% FBS, the transmittances of five groups of PTX-loaded liposomes were all higher than 91%, and no obvious aggregation of liposomes were found. The results indicated that these liposomes were stable enough for obtaining a longer half-life of blood *in vivo* [41].

3.6. Hemolysis assays

Hemocompatibility is a key factor to the application of liposomes *in vivo*. As shown in Fig. 5, with the increase of lipid concentration, the hemolysis rates of five groups of PTX-loaded liposomes were not significantly increased, and the hemolysis rate was still less than 10% even the lipid concentration was up to 400 μM, which indicated that PTX-loaded liposomes modified by biotin had good biosecurity. μ.

3.7. Cytotoxicity

In vitro cytotoxicity of different PTX-loaded liposomes against breast cancer cells and normal cells was performed by MTT assays. As shown in Fig. 6A and B, with the increase of paclitaxel concentration, the inhibition of PTX-Lip, PTX-Bio-Lip, PTX-Bio-Bio-Lip, PTX-tri-Bio-Lip and PTX-tetra-Bio-Lip on 4T1 and MCF-7 cells gradually increased. Compared with other types of PTX-loaded liposomes, PTX-tri-Bio-Lip modified by tri-Bio-Chol showed stronger cytotoxicity, especially for 4T1 cells. In addition, free paclitaxel showed better inhibitory activity, because the free drugs could enter the cell through passive diffusion directly and take effect without a drug release process, which indirectly indicated the sustained release of liposomes. As for normal cells (Fig. 6C), the cytotoxicity of different PTX-loaded liposomes against L929 cells was much weaker than breast cancer cells. And the biotin modified liposomes showed lower inhibition comparing with free PTX and non-modified liposomes, which may contribute to the selectivity between the biotin and SMVT receptors over-expressed on breast cancer cells.

3.8. Apoptosis assay

Annexin V-FITC/PI apoptosis detection kit was used to study the cell apoptosis induced by PTX-loaded liposomes. As shown in Fig. 7, the percentage of apoptosis and necrotic cells was 40.01 ± 1.98% for free PTX, 23.75 ± 2.85% for PTX-Lip, 25.55 ± 1.59% for PTX-Bio-Lip, 35.26 ± 1.68% for PTX-Bio-Bio-Lip, 43.29 ± 0.84% for PTX-tri-Bio-Lip and 36.84 ± 1.69% for PTX-tetra-Bio-Lip, respectively. Compared with other groups, PTX-tri-Bio-Lip modified by tri-Bio-Chol had a stronger effect on inducing apoptosis of 4T1 cells, which was consistent with the results of *in vitro* cytotoxicity.

3.9. Cellular uptake study

In order to primarily evaluate the selectivity, affinity and endocytosis of breast cancer cells for different branched biotin-modified liposomes, we measured the cellular uptake of CFPE-labeled liposomes on biotin receptor-positive cell line 4T1 cells and MCF-7 cells. As shown in Fig. 8A and B, both 4T1 cells and MCF-7 cells showed the strongest uptake capacity of tri-Bio-Lip modified by tri-Bio-Chol. On 4T1 cells, the fluorescence intensity of tri-Bio-Lip was 5.21 times of Lip, 2.60 times of Bio-Lip, 1.67 times of Bio-Bio-Lip and 1.17 times of tetra-Bio-Lip, respectively. The uptake of tri-Bio-Lip on MCF-7 cells was 2.90, 2.27, 1.70 and 1.33 times higher than that of Lip, Bio-Lip, Bio-Bio-Lip and tetra-Bio-Lip, respectively. As shown in Fig. 8C and D, the qualitative uptake experiment of laser confocal imaging showed that tri-Bio-Lip exhibited the highest uptake levels on 4T1 cells and MCF-7 cells, which was consistent with the quantitative results of flow cytometry.

By comparing the uptake of Lip, Bio-Lip, Bio-Bio-Lip, tri-Bio-Lip and tetra-Bio-Lip on 4T1 cells and MCF-7 cells, the results showed

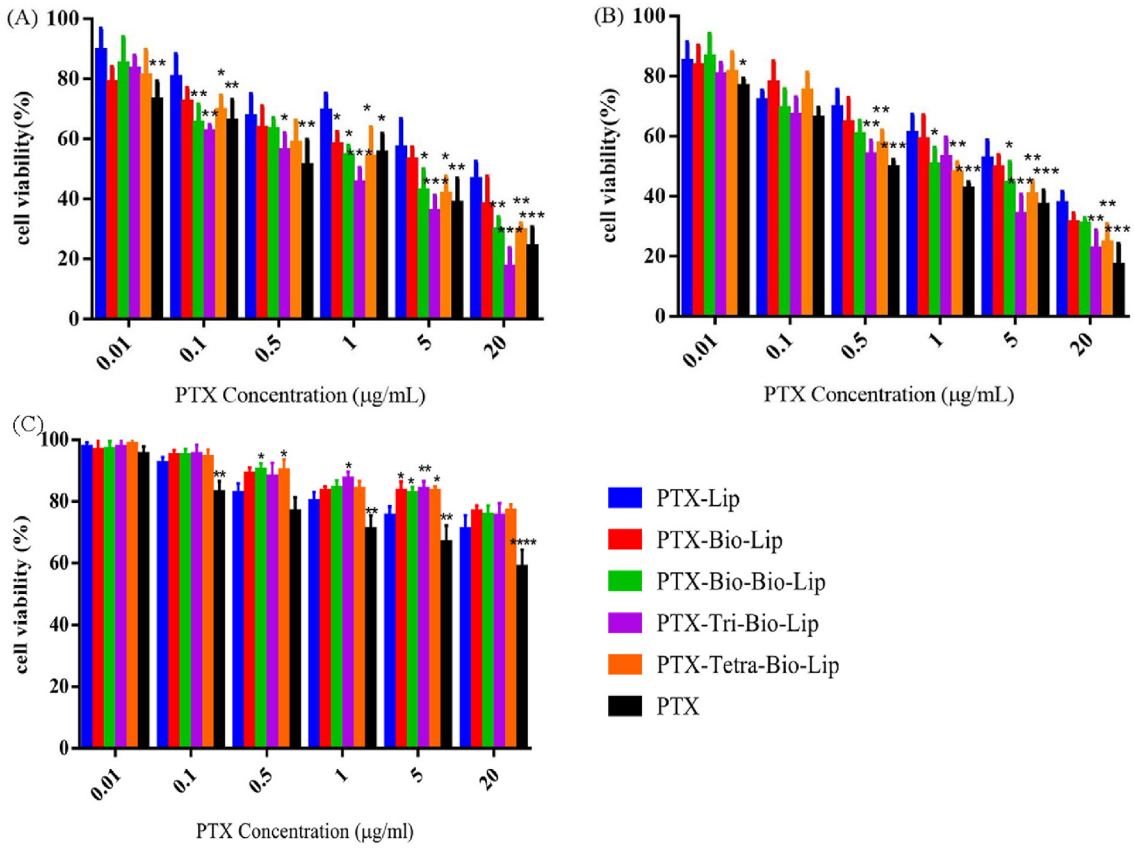

Fig. 6. (A) represents the cytotoxicity study of PTX-loaded liposomes and free PTX on 4T1 cells, (B) represents the cytotoxicity study of PTX-loaded liposomes and free PTX on MCF-7 cells; (C) represents the cytotoxicity study of PTX-loaded liposomes and free PTX on L929 cells; *, **, *** and **** represent $p < 0.05$, $p < 0.01$, $p < 0.001$ and $p < 0.0001$ versus PTX-Lip group, (mean ± SD, $n = 3$).

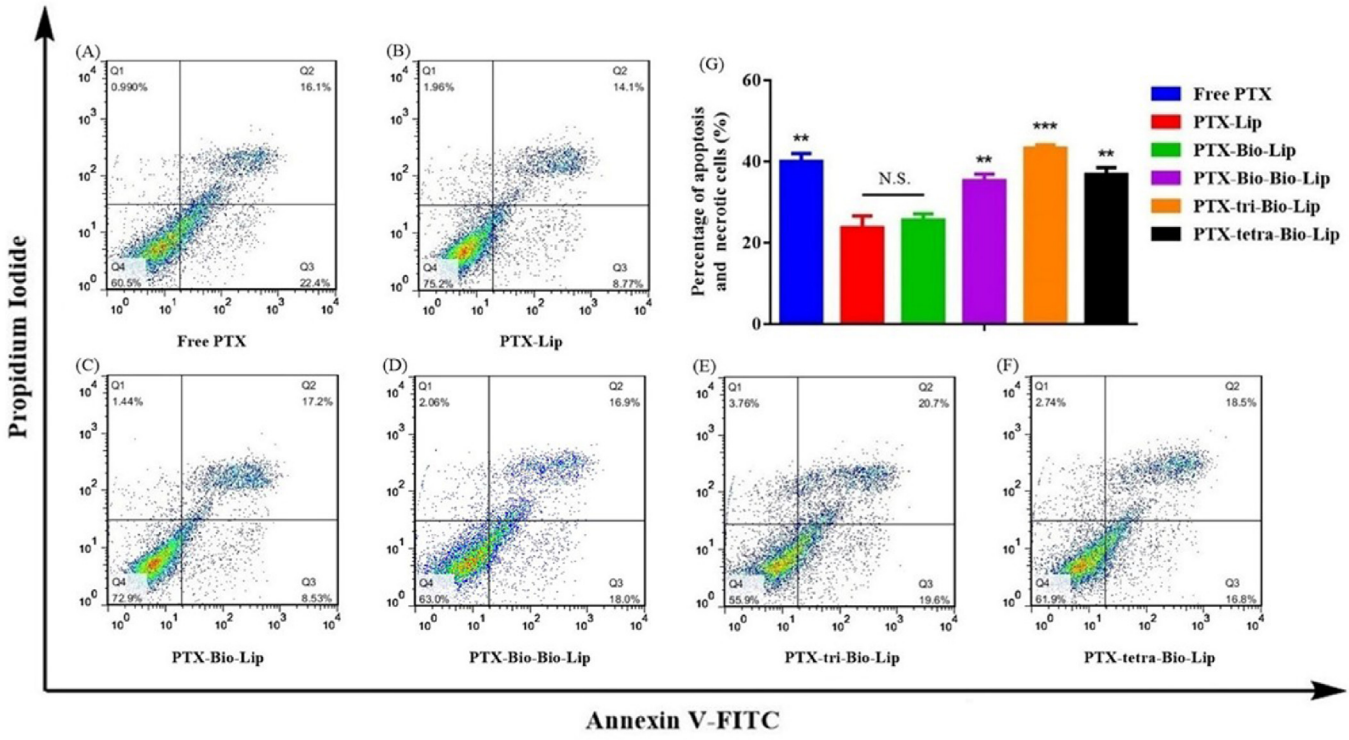

Fig. 7. (A), (B), (C), (D), (E) and (F) represent the apoptosis study of free paclitaxel, PTX-Lip, PTX-Bio-Lip, PTX-Bio-Bio-Lip, PTX-tri-Lip and PTX-tetra-Bio-Lip on 4T1 cells, respectively. (G) represents the percentage of apoptosis and necrotic cells after free PTX and PTX-loaded liposomes on 4T1 cells. **, *** represent $p < 0.01$ and $p < 0.001$ versus PTX-Lip group, respectively; N. S. indicates none significant difference, (mean ± SD, $n = 3$).

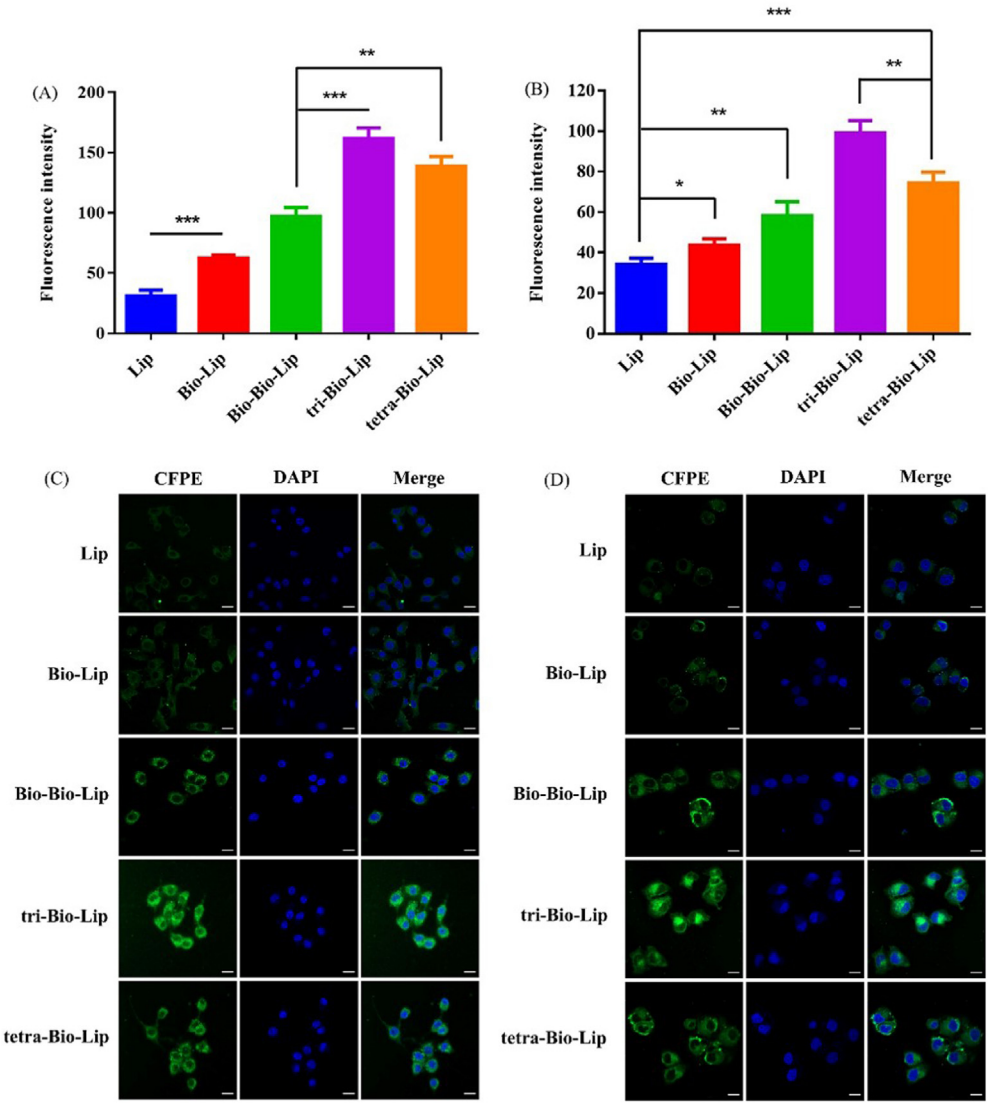

Fig. 8. (A) and (B) represent cellular uptake of CFPE-labeled liposomes determined by flow cytometer on 4T1 cells and MCF-7 cells, respectively; *, ** and *** represent $p < 0.05$, $p < 0.01$ and $p < 0.001$ versus Lip group, N. S. indicates none significant difference, (mean ± SD, n = 3). (C) and (D) represent cellular uptake of CFPE-labeled liposomes determined by CLSM on 4T1 cells and MCF-7 cells, respectively; green (CFPE-labeled liposomes), blue (DAPI stained nucleus), light blue (colocalized CFPE and DAPI), scale bars represent 20 μm, (mean ± SD, $n = 3$). (For interpretation of the references to color in this figure legend, the reader is referred to the Web version of this article.)

that the *in vitro* targeting ability of five groups of liposomes from strong to weak was tri-Bio-Lip > tetra-Bio-Lip > Bio-Bio-Lip > Bio-Lip > Lip. It can be seen that from single-branched biotin to tri-branched biotin-modified liposomes, increasing the density of targeting molecules can significantly enhance the targeting ability for breast cancer, which is consistent with our previous study [37]. But it was also found that tetra-Bio-Lip < tri-Bio-Lip, which was similar to other reports about the affinity between different branched ligands and receptors [36,42-44]. Thus, we concluded that in addition to targeting molecular density, the branching structure and spatial distance of biotin residues of ligands may also have an important influence on the affinity between liposomes modified by different branched biotin and SMVT receptor.

3.10. *In vivo* distribution and targeting

In our previous study [37], the distribution in plasma and tissues of PTX-Bio-Bio-Lip and PTX-Bio-Lip as well as the PTX-Lip were evaluated in 4T1 tumor-bearing BALB/c mice. The pharmacokinetic parameters of PTX in plasma showed the area under the concentration-time curve (AUC_{0-t}) of PTX in biotin modified liposomes were much higher than that of naked PTX within 24 h, meanwhile, the mean residence time (MRT) and the elimination half-life ($t_{1/2}$) of biotin modified liposomes was much longer comparing with the naked PTX and unmodified liposome. The results showed PTX-Bio-Bio-Lip and PTX-Bio-Lip possessed better blood circulation characteristics, which facilitated the liposomes to reach and deliver its cargo to the target site. Moreover, the distribution in tissues and tumors also showed the PTX-Bio-Bio-Lip accumulated more than other groups in the breast tumor. Based on these studies and the *in vitro* targeting results mentioned above in this study, we speculated that tri-Bio-lip and tetra-Bio-lip also have good blood circulation characteristics and stronger tumor targeting ability *in vivo*.

4T1 tumor-bearing BALB/c female mice were used to estimate the breast cancer targeting efficiency of liposomes modified by different branched biotin. As shown in Fig. 9A, *in vivo* image results showed that DiD-loaded liposomes modified by biotin accumulated

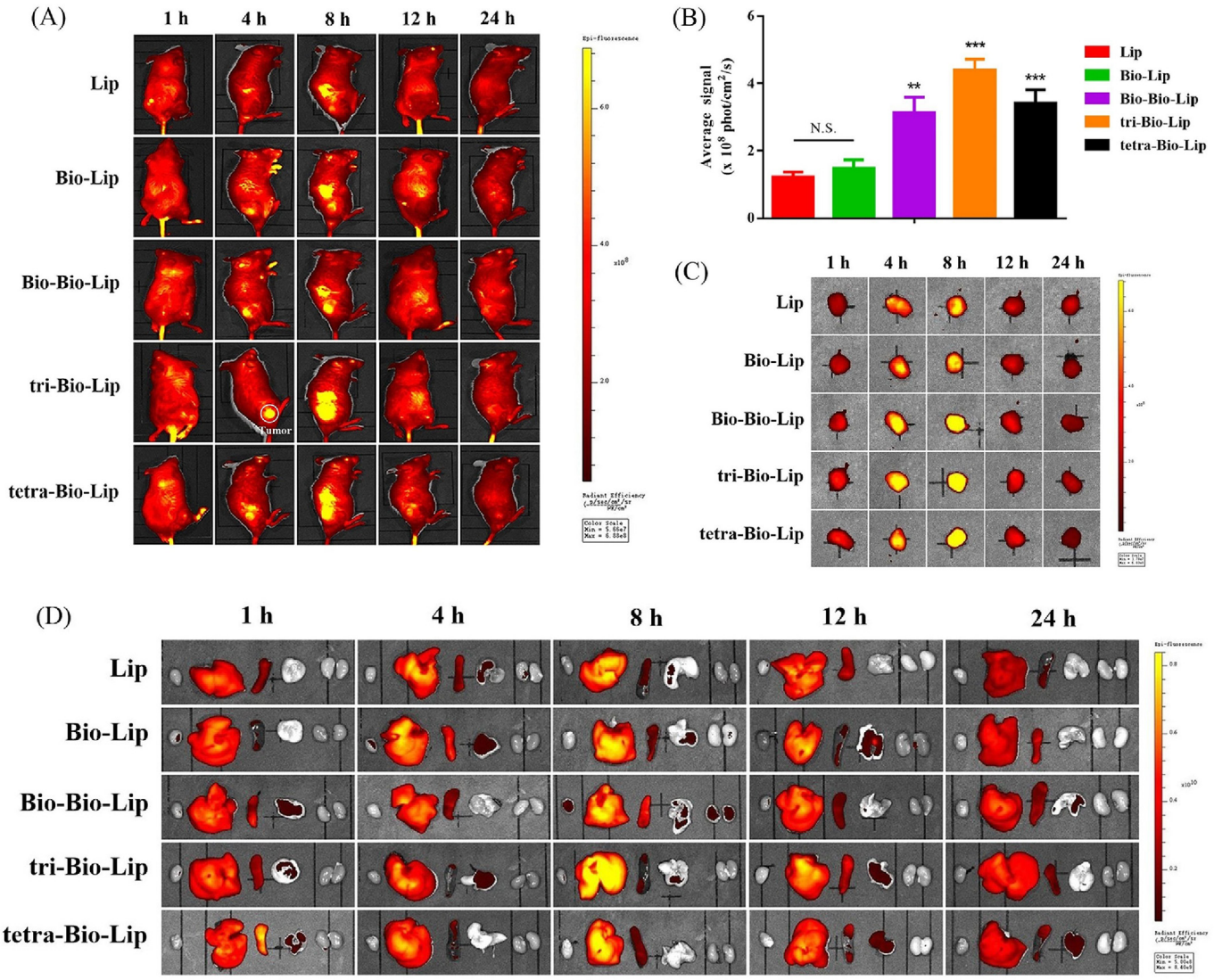

Fig. 9. (A) represents the imaging of different types of DiD-loaded liposomes in tumor-bearing mice, (B) represents the semi-quantitative fluorescence intensity analysis of different types of DiD-loaded liposomes in isolated tumor tissues 8 h after administration, (C) represents the imaging of different types of DiD-loaded liposomes in isolated tumor tissues, (D) represents the imaging of different types of DiD-loaded liposomes in isolated organs (from left to right are heart, liver, spleen, lung and kidney). **, *** represent $p < 0.01$ and $p < 0.001$ versus Lip group, respectively, N. S. indicates none significant difference, (mean ± SD, $n = 3$).

in tumor tissues 4 h after administration, with weak fluorescence intensity, and 8 h after administration reached the peak. As shown in Fig. 9C, *in vitro* image results of isolated tumor tissues showed that the fluorescence intensity of five groups of DiD-loaded liposomes reached its peak in tumor tissues 8 h after administration which was consistent with the results in Fig. 9A. As shown in Fig. 9B, the semi-quantitative results of fluorescence intensity of tumor tissues showed that the fluorescence intensity of tri-Bio-Lip was 3.59, 2.97, 1.40 and 1.29 times higher than that of Lip, Bio-Lip, Bio-Bio-Lip and tetra-Bio-Lip at 8 h, respectively. As shown in Fig. 9D, *in vitro* image results of isolated organs showed that five groups of DiD-loaded liposomes were mainly distributed in liver and spleen after administration, especially in liver.

The results of *in vivo* studies indicated that the *in vivo* targeting ability of five groups of liposomes from strong to weak was tri-Bio-Lip > tetra-Bio-Lip > Bio-Bio-Lip > Bio-Lip > Lip, which was consistent with the results of *in vitro* targeting studies. The *in vivo* studies further proved that increasing the density of targeting molecules of ligands can effectively enhance the breast cancer targeting ability of liposomes, and the branching structure and spatial distance of biotin residues of ligands may also have an important influence on the affinity between liposomes modified by different branched biotin and SMVT receptor.

Lee and other researchers have studied the affinity between different branched galactose (Gal)/N-acetylgalactosamine (GalNAc) residues and asialoglycoprotein receptor (ASGPR) [36,42-44]. The results showed that the affinity of different branched galactose residues with receptor were: tetra-branched galactoside > tri-branched galactoside ≫ bi-branched galactoside ≫ mono-galactoside, and the affinity of tri-branched galactoside with receptor was 50−100 times higher than that of mono-galactoside, but the affinity of tetra-branched galactoside with ASGPR was not significantly higher than that of tri-branched galactoside. Further research indicated that for the same bi-branched polysaccharides, the affinity of galactoside with ASGPR with the branching distance at 15 Å was higher than that of branching distance at 23 Å. The results of Biessen et al. [45] also showed that the affinity of galactoside with ASGPR was the strongest when the distance between

multi-branched galactoside was 20 Å, and the sequence of affinity from strong to weak was 20 Å ≫ 10 Å ≫ 4 Å. Therefore, combining with the results of these literatures, we analyzed that in addition to targeted molecular density, the branching structure and spatial distance of biotin residues of ligands may also have an important influence on the affinity between liposomes modified by different branched biotin and SMVT receptor.

Both the targeting evaluation *in vitro* and *in vivo* indicated tri-Bio-Lip can significantly improve the targeting ability of liposome for breast cancer, we speculated that PTX-tri-Bio-Lip could be a promising drug delivery system for the treatment of breast cancer. In our future studies, we would explore the impact of the branching structure and spatial distance of biotin residues on breast cancer targeting capacity and the therapeutic effect of tri-Bio-Lip for breast cancer.

4. Conclusion

In summary, a series of liposome ligands Bio-Chol, Bio-Bio-Chol, tri-Bio-Chol and tetra-Bio-Chol modified by different branched biotins were designed and synthesized in this study. And different types of liposomes Bio-Lip, Bio-Bio-Lip, tri-Bio-Lip and tetra-Bio-Lip with different targeting molecular density were prepared for targeting breast cancer. The cytotoxicity study and apoptosis assay of paclitaxel-loaded liposomes showed that PTX-tri-Bio-Lip had the strongest anti-proliferative effect on breast cancer cells. The cellular uptake studies on breast cancer cells indicated tri-Bio-Lip possessed the strongest internalization ability. Moreover, the *in vivo* image on 4T1 tumor-bearing BALB/c mice showed the enrichment of liposomes at tumor sites were tri-Bio-Lip > tetra-Bio-Lip > Bio-Bio-Lip > Bio-Lip > Lip. Both the targeting evaluation *in vitro* and *in vivo* indicated that increasing the density of targeting molecules of ligands can effectively enhance the breast cancer targeting ability of liposomes. Besides, the branching structure and spatial distance of biotin residues may also have an important influence on the affinity between liposomes modified by different branched biotin and SMVT receptors. Among these liposome ligands, tri-Bio-Chol can significantly improve the targeting ability of liposome for breast cancer, making it a potential breast cancer targeting ligand. This study not only enhances the targeting ability of biotin for breast cancer, but also makes a great difference to further targeting drug delivery system.

Declaration of competing interest

The authors declare no competing financial interest.

Acknowledgement

This work was supported by the National Natural Science Foundation of China (No. 81573286, No. 81773577 & No. 81903448), the Sichuan Science and Technology Program (2018JY0537), the Fundamental Research Funds for the Central Universities (2012017yjsy211) and the Open Research Subject of Healthy, Xihua University (szjj2017-036).

Appendix A. Supplementary data

Supplementary data to this article can be found online at https://doi.org/10.1016/j.ejmech.2020.112204.

References

[1] R.L. Siegel, K.D. Miller, A. Jemal, Cancer statistics, 2019, CA A Cancer J. Clin. 69 (1) (2019) 7–34, https://doi.org/10.3322/caac.21551.
[2] Tracy-Ann, Rachel Moo, et al., Overview of breast cancer therapy, Pet. Clin. 13 (3) (2018) 339–354, https://doi.org/10.1016/j.cpet.2018.02.006.
[3] X. Tang, W.S. Loc, C. Dong, et al., The use of nanoparticulates to treat breast cancer, Nanomedicine 12 (19) (2017) 2367–2388, https://doi.org/10.2217/nnm-2017-0202.
[4] W. Di, S. Mengjie, X. Hui-Yi, et al., Nanomedicine applications in the treatment of breast cancer: current state of the art, Int. J. Nanomed. 12 (2017) 5879–5892, https://doi.org/10.2147/IJN.S123437.
[5] I. Brigger, C. Dubernet, P. Couvreur, Nanoparticles in cancer therapy and diagnosis, Adv. Drug Deliv. Rev. 64 (supp_S) (2012) 24–36, https://doi.org/10.1016/j.addr.2012.09.006.
[6] C. Oerlemans, W. Bult, M. Bos, et al., Polymeric micelles in anticancer therapy: targeting, imaging and triggered release, Pharmaceut. Res. 27 (12) (2010) 2569–2589, https://doi.org/10.1007/s11095-010-0233-4.
[7] Saeedi Majid, Masoumeh, et al., Applications of nanotechnology in drug delivery to the central nervous system, Biomed. Pharmacother. 111 (2019) 666–675, https://doi.org/10.1016/j.biopha.2018.12.133.
[8] H. Su, Y. Wang, S. Liu, et al., Emerging transporter-targeted nanoparticulate drug delivery systems, Acta Pharm. Sin. B 9 (1) (2018) 49–58, https://doi.org/10.1016/j.apsb.2018.10.005.
[9] P. Senthil Kumar, I. Pastoriza-Santos, B. Rodríguez-González, et al., High-yield synthesis and optical response of gold nanostars, Nanotechnology 19 (1) (2008), 015606, https://doi.org/10.1088/0957-4484/19/01/015606.
[10] S. Mura, J. Nicolas, P. Couvreur, Stimuli-responsive nanocarriers for drug delivery, Nat. Mater. 12 (11) (2013) 991–1003, https://doi.org/10.1038/nmat3776.
[11] M. Shubhangi, P. Abhimanyu, K. Kaushik, et al., Functionalized carbon nanotubes as emerging delivery system for the treatment of cancer, Int. J. Pharm. 548 (1) (2018) 540–558, https://doi.org/10.1016/j.ijpharm.2018.07.027.
[12] S. Mitra, H.S. Sasmal, T. Kundu, et al., Targeted drug delivery in covalent organic nanosheets (CONs) via sequential postsynthetic modification, J. Am. Chem. Soc. 139 (12) (2017) 4513–4520, https://doi.org/10.1021/jacs.7b00925.
[13] H.D.D. Lee, J.W. Ha, J. Yue, T.W. Odom, Enhanced human epidermal growth factor receptor 2 degradation in breast cancer cells by lysosome-targeting gold nanoconstructs, ACS Nano 9 (10) (2015) 9859–9867, https://doi.org/10.1021/acsnano.5b05138.
[14] Y. Malam, M. Loizidou, A.M. Seifalian, Liposomes and nanoparticles: nanosized vehicles for drug delivery in cancer, Trends Pharmacol. Sci. 30 (11) (2009) 592–599, https://doi.org/10.1021/acsnano.5b05138.
[15] C. Heneweer, S.E. Gendy, O. Penate-Medina, Liposomes and inorganic nanoparticles for drug delivery and cancer imaging, Ther. Deliv. 3 (5) (2012) 645–656, https://doi.org/10.4155/tde.12.38.
[16] S. Naz, M. Shamoon, R. Wang, et al., Advances in therapeutic implications of inorganic drug delivery nano-platforms for cancer, Int. J. Mol. Sci. 20 (4) (2019) 965, https://doi.org/10.3390/ijms20040965.
[17] A. Kumari, S.K. Yadav, S.C. Yadav, Biodegradable polymeric nanoparticles based drug delivery systems, Colloids Surf. B Biointerfaces 75 (1) (2010) 1–18, https://doi.org/10.1016/j.colsurfb.2009.09.001.
[18] P. Evelyn Roopngam, Liposome and polymer-based nanomaterials for vaccine applications, Nanomed. J. 6 (1) (2019) 1–10, https://doi.org/10.22038/nmj.2019.06.001.
[19] Y. Cheng, Y. Ji, RGD-modified polymer and liposome nanovehicles: recent research progress for drug delivery in cancer therapeutics, Eur. J. Pharmaceut. Sci. 128 (2019) 8–17, https://doi.org/10.1016/j.ejps.2018.11.023.
[20] T.M. Allen, P.R. Cullis, Liposomal drug delivery systems: from concept to clinical applications, Adv. Drug Deliv. Rev. 65 (1) (2013) 36–48, https://doi.org/10.1016/j.addr.2012.09.037.
[21] N. Van Rooijen, A. Sanders, Liposome mediated depletion of macrophages: mechanism of action, preparation of liposomes and applications, J. Immunol. Methods 174 (1–2) (1994) 83–93, https://doi.org/10.1016/0022-1759(94)90012-4.
[22] H. He, Y. Lu, J. Qi, et al., Biomimetic thiamine- and niacin-decorated liposomes for enhanced oral delivery of insulin, Acta Pharm. Sin. B 8 (1) (2018) 97–105, https://doi.org/10.1016/j.apsb.2017.11.007.
[23] Y. Zhong, F. Meng, C. Deng, et al., Ligand-directed active tumor-targeting polymeric nanoparticles for cancer chemotherapy, Biomacromolecules 15 (6) (2014) 1955–1969, https://doi.org/10.1021/bm5003009.
[24] T. Dai, K. Jiang, W. Lu, Liposomes and lipid disks traverse the BBB and BBTB as intact forms as revealed by two-step Forster resonance energy transfer imaging, Acta Pharm. Sin. B 8 (2) (2018) 261–271, https://doi.org/10.1016/j.apsb.2018.01.004.
[25] H. Chen, X. Wei, J. Qin, et al., Synthesis, characterization and in vivo efficacy of biotin-conjugated pullulan acetate nanoparticles as a novel anticancer drug carrier, J. Biomed. Nanotechnol. 13 (9) (2017) 1134–1146, https://doi.org/10.1166/jbn.2017.2402.
[26] N. Nateghian, N. Goodarzi, M. Amini, et al., Biotin/Folate-decorated human serum albumin nanoparticles of docetaxel: comparison of chemically conjugated nanostructures and physically loaded nanoparticles for targeting of breast cancer, Chem. Biol. Drug Des. 87 (1) (2016) 69–82, https://doi.org/10.1111/cbdd.12624.
[27] H. Chen, L.Q. Xie, J. Qin, et al., Surface modification of PLGA nanoparticles with biotinylated chitosan for the sustained in vitro release and the enhanced cytotoxicity of epirubicin, Colloids Surf. B Biointerfaces 138 (2016) 1–9, https://doi.org/10.1016/j.colsurfb.2015.11.033.
[28] S. Collina, New perspectives in cancer therapy: the biotin-antitumor molecule

conjugates, Med. Chem. 8 (2014) 1–4, https://doi.org/10.4172/2161-0444.s1-004.
[29] A.D. Vadlapudi, R.K. Vadlapatla, A.K. Mitra, Sodium dependent multivitamin transporter (SMVT): a potential target for drug delivery, Curr. Drug Targets 13 (7) (2012) 994–1003, https://doi.org/10.2174/138945012800675650.
[30] S. Chen, X. Zhao, J. Chen, et al., Mechanism-Based tumor-targeting drug delivery system. Validation of efficient vitamin receptor-mediated endocytosis and drug release, Bioconjugate Chem. 21 (5) (2010) 979–987, https://doi.org/10.1021/bc9005656.
[31] J.F. Shi, P. Wu, Z.H. Jiang, et al., Synthesis and tumor cell growth inhibitory activity of biotinylated annonaceous acetogenins, Eur. J. Med. Chem. 71 (2014) 219–228, https://doi.org/10.1016/j.ejmech.2013.11.012.
[32] G. Russell-Jones, K. McTavish, J. McEwan, et al., Vitamin-mediated targeting as a potential mechanism to increase drug uptake by tumours, J. Inorg. Biochem. 98 (10) (2004) 1625–1633, https://doi.org/10.1016/j.jinorgbio.2004.07.009.
[33] I. Poudel, R. Ahiwale, A. Pawar, et al., Development of novel biotinylated chitosan-decorated docetaxel-loaded nanocochleates for breast cancer targeting, Artif. Cells Nanomed. Biotechnol. (2018) 1–12, https://doi.org/10.1080/21691401.2018.1453831.
[34] B. Qu, X. Li, M. Guan, et al., Design, synthesis and biological evaluation of multivalent glucosides with high affinity as ligands for brain targeting liposomes, Eur. J. Med. Chem. 72 (2014) 110–118, https://doi.org/10.1016/j.ejmech.2013.10.007.
[35] Z. Guo, B. He, H. Jin, et al., Targeting efficiency of RGD-modified nanocarriers with different ligand intervals in response to integrin αvβ3 clustering, Biomaterials 35 (23) (2014) 6106–6117, https://doi.org/10.1016/j.biomaterials.2014.04.031.
[36] T.P. Prakash, J. Yu, M.T. Migawa, et al., Comprehensive structure–activity relationship of TriantennaryN-acetylgalactosamine conjugated antisense oligonucleotides for targeted delivery to hepatocytes, J. Med. Chem. 59 (6) (2016) 2718–2733, https://doi.org/10.1021/acs.jmedchem.5b01948.
[37] R. Lu, L. Zhou, Q. Yue, et al., Liposomes modified with double-branched biotin: a novel and effective way to promote breast cancer targeting, Bioorg. Med. Chem. 27 (14) (2019) 3115–3127, https://doi.org/10.1016/j.bmc.2019.05.039.
[38] Y. Pu, H. Zhang, Y. Peng, et al., Dual-targeting liposomes with active recognition of GLUT5 and alphavbeta3 for triple-negative breast cancer, Eur. J. Med. Chem. 183 (2019) 111720, https://doi.org/10.1016/j.ejmech.2019.111720.
[39] Y. Wang, L. Chen, L. Tan, et al., PEG-PCL based micelle hydrogels as oral docetaxel delivery systems for breast cancer therapy, Biomaterials 35 (25) (2014) 6972–6985, https://doi.org/10.1016/j.biomaterials.2014.04.099.
[40] S. Rojas, J.D. Gispert, R. Martín, et al., Biodistribution of amino-functionalized diamond nanoparticles. In vivo studies based on 18F radionuclide emission, ACS Nano 5 (7) (2011) 5552–5559, https://doi.org/10.1021/nn200986z.
[41] B. Jang, J.-Y. Park, C.-H. Tung, et al., Gold nanorod-photosensitizer complex for near-infrared fluorescence imaging and photodynamic/photothermal therapy in vivo, ACS Nano 5 (2) (2011) 1086–1094, https://doi.org/10.1021/nn102722z.
[42] G.A. Kinberger, T.P. Prakash, J. Yu, et al., Conjugation of mono and di-GalNAc sugars enhances the potency of antisense oligonucleotides via ASGR mediated delivery to hepatocytes, Bioorg. Med. Chem. Lett 26 (15) (2016) 3690–3693, https://doi.org/10.1016/j.bmcl.2016.05.084.
[43] Y. Lee, R.R. Townsend, M.R. Hardy, et al., Binding of synthetic oligosaccharides to the hepatic Gal/GalNAc lectin, J. Biol. Chem. 258 (1) (1983) 199–202.
[44] P.C.N. Rensen, L.A.J.M. Sliedregt, M. Ferns, et al., Determination of the upper size limit for uptake and processing of ligands by the asialoglycoprotein receptor on hepatocytesin vitro and in vivo, J. Biol. Chem. 276 (40) (2001) 37577–37584, https://doi.org/10.1074/jbc.M101786200.
[45] E.A.L. Biessen, D.M. Beuting, H.C.P.F. Roelen, et al., Synthesis of cluster galactosides with high affinity for the hepatic asialoglycoprotein receptor, J. Med. Chem. 38 (9) (1995) 1538–1546, https://doi.org/10.1021/jm00009a014.